Acta Mech 223, 705–720 (2012)
DOI 10.1007/s00707-011-0586-8

Y. Z. Chen

Numerical solution of elastic inclusion problem using complex variable boundary integral equation

Received: 5 June 2011 / Revised: 7 November 2011 / Published online: 20 December 2011

Abstract Based on a complex variable boundary integral equation (CVBIE) suggested previously, this paper provides a numerical solution for the elastic inclusion problem using CVBIE. A dissimilar elastic inclusion is embedded in the infinite matrix. The original problem is decomposed into two problems. One is an interior boundary value problem (BVP) for the elastic inclusion, while the other is an exterior BVP for the matrix with notch. Both problems are connected by conventional boundary integral equations (BIEs) in complex variables. After performing discretization for the coupled BIEs, the inverse matrix technique is suggested to solve the relevant algebraic equations. Based on the properties of some integral operators, three ways for the inverse matrix technique are suggested. Several numerical examples are carried out to prove the efficiency of the suggested method.

1 Introduction

In composite materials, the matrix may be reinforced by some elastic inclusions with different elastic properties. Physically, under the action of loading, the stress distributions are generally not uniform in the inclusion problem, particularly, in the place near the interface boundary. In plane elasticity, though the governing equations for the matrix and the inclusion are same. However, since the elastic constants are different for the matrix and the inclusion, the final solution must depend on the elastic constants and the continuation conditions along the interface. Therefore, the solution technique for the inclusion problem must be complicated. In addition, the inclusion problem may generally be decomposed into two boundary value problems (BVPs). Among them, one is the interior BVP and other is the exterior BVP. It is known that the properties of some integration operators in the interior and exterior BVPs may have some differences. This point should be considered in the formulation of boundary integral equations for the interior and exterior BVPs.

A lot of research work has been devoted to the elastic inclusion in plane elasticity. A solution was presented for determining the stresses in an infinite elastic plate containing a rectangular inclusion subjected to a uniform stress field [1]. The solution depends on the conformal mapping functions for an interior region and an exterior region. A boundary-domain integral equation in elastic inclusion problems was introduced [2]. In the formulation, the displacement integral equation is applied to all the boundary nodes, and the strain integral equation is used at all the collocation nodes of inclusions. Different integral equation approaches were suggested to the elastic half-plane problem with inclusions [3]. A new integral equation formulation of two-dimensional infinite isotropic medium with various inclusions and cracks was presented in [4]. The derivation depends on some expressions for displacements and tractions at domain point.

A numerical method for solving the problem of an isotropic elastic half-plane containing many circular elastic inclusions was proposed in [5]. The derivation was based on the complex variable hypersingular integral

Y. Z. Chen (✉)
Division of Engineering Mechanics, Jiangsu University, Zhenjiang 212013, Jiangsu, People's Republic of China
E-mail: chens@ujs.edu.cn
Tel.: +086-511-88780780

equation. The numerical solution was mainly devoted to the circular inclusions where the traction component is approximated by complex Fourier series representation. Faber series method for plane problems of an arbitrarily shaped inclusion was suggested [6]. In the paper, the complex potentials in the form of the Faber series are used for the elastic inclusion and the derivation depends on the conformal mapping of contours. A systematic approach was proposed to calculate the torsional rigidity and stress of a circular bar containing multiple circular inclusions [7]. The formulation is based on the null-field integral approach.

It is felt that the inclusion problem had not been solved very well previously. For example, in some referenced papers, the inclusion has a limitation of circular shape and some solutions depend on the conformal mapping function.

Based on a complex variable boundary integral equation (CVBIE) suggested previously [8], this paper provides a numerical solution for elastic inclusion problem using CVBIE. In the original problem, a dissimilar elastic inclusion is embedded in the infinite matrix. The original problem is decomposed into two problems. One is an interior boundary value problem (BVP) for the elastic inclusion, while the other is an exterior boundary value problem for the matrix with notch. Both problems are connected by conventional boundary integral equations. After performing discretization for the coupled BIEs, the inverse matrix technique is suggested to solve the relevant algebraic equations. Based on the properties of some integral operators, three ways for the inverse matrix technique are used. The purpose for the suggested three variations of substitution is to provide flexibility in the numerical solution. In the derivation, the configuration of the interface boundary is arbitrary. Several numerical examples are carried out to prove the efficiency of the suggested method. In the examples, the ratio of the two shear modulus of elasticity changes from near 0 (10^{-5}), 0.1, 0.5, 1, 2–10.

2 Analysis

The analysis presented below mainly depends on two kinds of integral equation. Therefore, the boundary integral equations for interior region and exterior region are introduced. Both of them are presented in the complex variable form [8]. Properties of some integration operators are introduced, which are useful in the analysis. Formulation of the elastic inclusion problem based on the coupled integral equations is proposed. After discretization of the BIEs, three ways using the inverse matrix technique are suggested to obtain the final numerical solution. For the case of a concentrated force applied on the inclusion, the relevant scheme for solution is also proposed.

2.1 Complex variable boundary integral equations for interior region and exterior region

Recently, a boundary integral equation for an interior region using complex variable was suggested [8], which is equivalent to the formulation based on real variable [9,10]. Some relevant formulations based on complex variables can be referred to [11–17]. The suggested BIE is more straightforward, since all involved arguments are expressed in an explicit form.

After some manipulation, the boundary integral equation for the interior problem takes the following form [8] (Fig. 1a)

$$\frac{U(t_o)}{2} + B_1 i \int_\Gamma \left(\frac{\kappa - 1}{t - t_o} U(t)\mathrm{d}t - L_1(t, t_o)U(t)\mathrm{d}t + L_2(t, t_o)\overline{U(t)}\mathrm{d}t \right)$$
$$= B_2 i \int_\Gamma \left(2\kappa \ln|t - t_o|\, Q(t)\mathrm{d}t + \frac{t - t_o}{\bar{t} - \bar{t}_o}\overline{Q(t)}\mathrm{d}\bar{t} \right), \quad (t_o \in \Gamma, \text{ for the interior problem}), \tag{1}$$

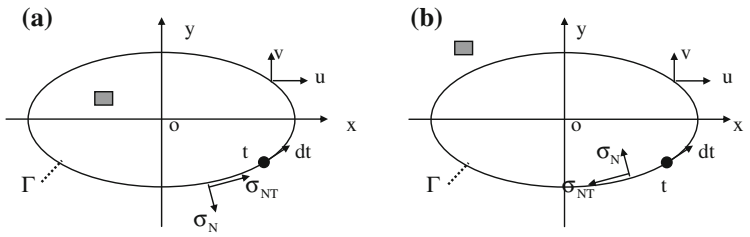

Fig. 1 **a** Interior boundary value problem, **b** exterior boundary value problem, *filled rectangle* region defined

where Γ denotes the boundary of the interior region. In Eq. (1), $U(t)$ and $Q(t)$ denote the displacement and traction along the boundary, which are defined by

$$U(t) = u(t) + \mathrm{i}v(t),\ Q(t) = \sigma_N(t) + \mathrm{i}\,\sigma_{NT}(t), \qquad (t \in \Gamma). \tag{2}$$

In addition, two elastic constants and two kernels are defined by

$$B_1 = \frac{1}{2\,\pi(\kappa+1)}, \quad B_2 = \frac{1}{4\,\pi\,G(\kappa+1)}, \tag{3}$$

$$\begin{aligned} L_1(t,\tau) &= -\frac{\mathrm{d}}{\mathrm{d}t}\left\{\ln\frac{t-\tau}{\bar{t}-\bar{\tau}}\right\} = -\frac{1}{t-\tau} + \frac{1}{\bar{t}-\bar{\tau}}\frac{\mathrm{d}\bar{t}}{\mathrm{d}t}, \\ L_2(t,\tau) &= \frac{\mathrm{d}}{\mathrm{d}t}\left\{\frac{t-\tau}{\bar{t}-\bar{\tau}}\right\} = \frac{1}{\bar{t}-\bar{\tau}} - \frac{t-\tau}{(\bar{t}-\bar{\tau})^2}\frac{\mathrm{d}\bar{t}}{\mathrm{d}t}, \end{aligned} \tag{4}$$

where $\kappa = 3-4\nu$ (for plane strain condition), $\kappa = (3-\nu)/(1+\nu)$ (for plane stress condition), G is the shear modulus of elasticity, and ν is the Poisson's ratio. In this paper, the plane strain condition and $\nu = 0.3$ are assumed. In Eq. (1), the increment "dt" is going forward in an anticlockwise direction.

Generally, if one uses the BIE shown by Eq. (1) to an exterior boundary value problem, the increment "dt" should be going forward in a clockwise direction. However, it is preferable to define increment "dt" in the anticlockwise direction. In the case for the exterior boundary value problem (Fig. 1b), from Eq. (1), the relevant BIE should be written as

$$\begin{aligned} &\frac{U(t_o)}{2} - B_1 i \int_\Gamma \left(\frac{\kappa-1}{t-t_o}U(t)\mathrm{d}t - L_1(t,t_o)U(t)\mathrm{d}t + L_2(t,t_o)\overline{U(t)}\mathrm{d}t\right) \\ &\quad = -B_2 i \int_\Gamma \left(2\,\kappa\ln|t-t_o|\,Q(t)\mathrm{d}t + \frac{t-t_o}{\bar{t}-\bar{t}_o}\overline{Q(t)}\mathrm{d}\bar{t}\right), \quad (t_o \in \Gamma,\ \text{for exterior problem}). \end{aligned} \tag{5}$$

Note that in Eqs. (1) and (5), the portions for integration just differ by a factor -1.

The above-mentioned BIEs are formulated for a general case with two elastic constants "G" and "ν". Suppose that the BIE is used for an interior region, or for an inclusion in Example 1 cited below, and the inclusion has two elastic constants G_1 and ν_1. In this case, the elastic constants G and ν involved in Eqs. (1) and (3) and some place should be replaced by G_1 and ν_1 accordingly.

Properties for some integration operators are introduced below. The left-hand term of Eq. (1) is defined as an integration operator as follows:

$$(K_{\mathrm{in}}U)(t_o) = \frac{U(t_o)}{2} + B_1 i \int_\Gamma \left(\frac{\kappa-1}{t-t_o}U(t)\mathrm{d}t - L_1(t,t_o)U(t)\mathrm{d}t + L_2(t,t_o)\overline{U(t)}\mathrm{d}t\right) \tag{6a}$$

or

$$(K_{\mathrm{in}}U)(t_o) = \frac{1}{2}\int_\Gamma \delta(t-t_o)U(t)\mathrm{d}t + B_1 i \int_\Gamma \left(\frac{\kappa-1}{t-t_o}U(t)\mathrm{d}t - L_1(t,t_o)U(t)\mathrm{d}t + L_2(t,t_o)\overline{U(t)}\mathrm{d}t\right), \tag{6b}$$

where $\delta(t-t_o)$ denotes the Dirac function.

Similarly, the left-hand term of Eq. (5) is defined as an integration operator as follows:

$$(K_{\mathrm{ex}}U)(t_o) = \frac{U(t_o)}{2} - B_1 i \int_\Gamma \left(\frac{\kappa-1}{t-t_o}U(t)\mathrm{d}t - L_1(t,t_o)U(t)\mathrm{d}t + L_2(t,t_o)\overline{U(t)}\mathrm{d}t\right) \tag{7a}$$

or

$$(K_{\mathrm{ex}}U)(t_o) = \frac{1}{2}\int_\Gamma \delta(t-t_o)U(t)\mathrm{d}t - B_1 i \int_\Gamma \left(\frac{\kappa-1}{t-t_o}U(t)\mathrm{d}t - L_1(t,t_o)U(t)\mathrm{d}t + L_2(t,t_o)\overline{U(t)}\mathrm{d}t\right). \tag{7b}$$

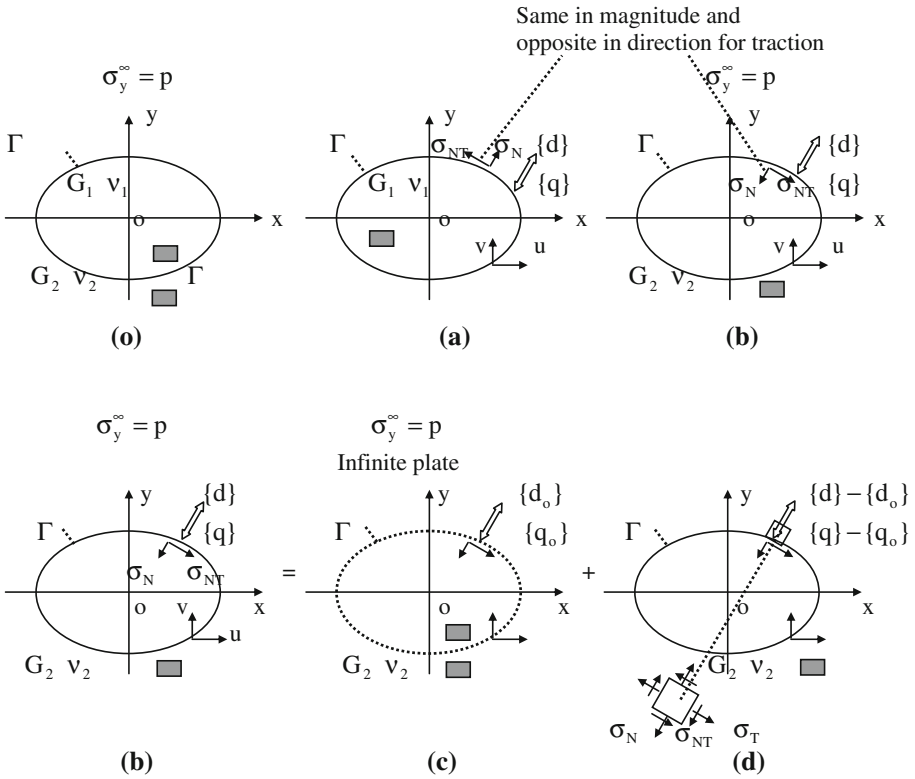

Fig. 2 An infinite plate with an elastic inclusion and remote loading $\sigma_y^\infty = p$, **o** the original problem, **a** an interior BVP, **b** an exterior BVP, **c** a homogenous infinite plate with remote loading $\sigma_y^\infty = p$, **d** an particular exterior BVP (where (**b**) = (**c**)+(**d**)), *filled rectangle* region defined

In the meantime, we define three displacement modes along the boundary as follows:

$$U_1(t) = 1, \quad (\text{or } u = 1,\ v = 0,\ \text{for } t \in \Gamma), \tag{8a}$$

$$U_2(t) = i, \quad (\text{or } u = 0,\ v = 1,\ \text{for } t \in \Gamma), \tag{8b}$$

$$U_3(t) = it, \quad (\text{or } u = -y_t,\ v = x_t,\ \text{with } t = x_t + \mathrm{i}y_t,\ \text{for } t \in \Gamma). \tag{8c}$$

Clearly, $U_i(t)$ $(i = 1, 2, 3)$ represent three rigid motions for the boundary $t \in \Gamma$. It has been proved that we have the following important properties [18]

$$(K_{\text{in}}U)(t_o)|_{U(t)=U_i(t)} = 0, \quad (i = 1, 2, 3), \tag{9}$$

$$(K_{\text{ex}}U)(t_o)|_{U(t)=U_i(t)} = U_i(t_o), \quad (i = 1, 2, 3). \tag{10}$$

From Eqs. (9) and (10), we see that two integration operators $(K_{\text{in}}U)(t_o)$ and $(K_{\text{ex}}U)(t_o)$ have quite different property. The properties shown by Eqs. (9) and (10) are useful in the following derivation.

2.2 Formulation of the elastic inclusion problem based on the integral equations

The original problem for an elastic inclusion is shown by Fig. 2o, where the inclusion and matrix have the elastic constants G_1, ν_1 and G_2, ν_2 (the shear modulus of elasticity and the Poisson's ratio), respectively. The remote loading is denoted by $\sigma_y^\infty = p$.

The original problem shown by Fig. 2o can be decomposed into two boundary value problems (Fig. 2a, b). Among them, one is interior BVP shown by Fig. 2a and the other is the exterior BVP shown by Fig. 2b.

In Fig. 2, two vectors along the boundary are defined by

$$\{d\} = \{u_1 v_1 \dots u_j v_j \dots u_M v_M\}^T, \tag{11}$$

$$\{q\} = \{\sigma_{N,1}\, \sigma_{NT,1} \dots \sigma_{N,j}\, \sigma_{NT,j} \dots \sigma_{N,M}\, \sigma_{NT,M}\}^T. \tag{12}$$

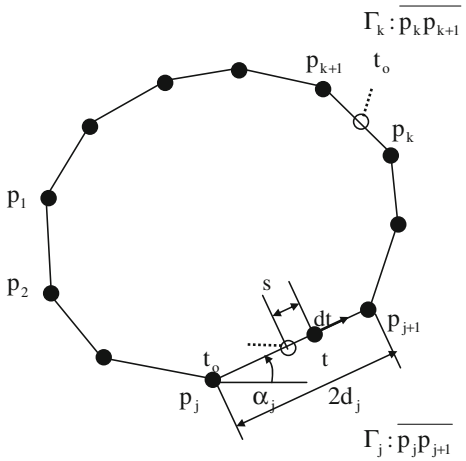

Fig. 3 Boundary elements for an interior boundary value problem

The vector $\{d\}$ is defined by many displacement components (u_j v_j) along the boundary Γ. Similarly, the vector $\{q\}$ is defined by many traction components ($\sigma_{N,j}$ $\sigma_{NT,j}$) along the boundary Γ (Fig. 2). Clearly, from the continuation condition of displacements and reciprocal property of tractions along interface boundary, the same vectors $\{d\}$ and $\{q\}$ are applied along the boundaries in Fig. 2a and b.

In addition, the exterior BVP by Fig. 2b can be considered as a superposition of two problems shown by Fig. 2c, d. In problem shown by Fig. 2c, a homogenous infinite plate is stretched by tension $\sigma_y^\infty = p$. In this case, two vectors $\{d_o\}$ and $\{q_o\}$ are applied along the boundary in Fig. 2c, which are easy to evaluate. Clearly, two vectors $\{d\} - \{d_o\}$ and $\{q\} - \{q_o\}$ are applied along the boundary in Fig. 2d. In the problem shown by Fig. 2d, the remote traction is vanishing (or $\sigma_y^\infty = 0$). Thus, we can use the conventional BIE for the problem shown in Fig. 2d accordingly.

For the interior problem shown in Fig. 2a, after discretization of Eq. (1), the relevant BIE can be reduced to the following form

$$[\mathbf{D}_1]\{d\} = \quad [\mathbf{Q}_1]\{q\}. \tag{13}$$

It is seen that two matrices $[\mathbf{D}_1]$ and $[\mathbf{Q}_1]$ are formulated based on Eq. (1) and two elastic constants G_1 and ν_1.

A compact explanation for the descretization of Eq. (1) is introduced below. In the descretization, the contour is approximated by many boundary line elements (Fig. 3). The observation point t_o is generally placed at the middle point of the interval $\overline{p_j p_{j+1}}$ ($j = 1, 2, \ldots$) (Fig. 3). In addition, a constant density function for $U(t)$ and $Q(t)$ is assumed on the interval $\overline{p_j p_{j+1}}$ ($j = 1, 2, \ldots$). In this case, we will meet two cases of integration in the process of discretization.

In the first case, t_o is placed at the middle point of the interval $\overline{p_j p_{j+1}}$ and integration is performed along $\overline{p_j p_{j+1}}$ denoting by Γ_j. For the left-hand side of Eq. (1), in the condition of $U(t)$ being constant along Γ_j, we have (Fig. 3)

$$I_1 = \int_{\Gamma_j} \frac{\mathrm{d}t}{t - t_o} = \int_{-d_j}^{d_j} \frac{\mathrm{d}s}{s} = 0, \quad (\text{for } t_o \text{ at middle point of } \overline{p_j p_{j+1}}), \tag{14}$$

$$I_2 = \int_{\Gamma_j} L_1(t, t_o)\mathrm{d}t = 0, \quad (\text{for } t_o \text{ at middle point of } \overline{p_j p_{j+1}}), \tag{15}$$

$$I_3 = \int_{\Gamma_j} L_2(t, t_o)\mathrm{d}t = 0, \quad (\text{for } t_o \text{ at middle point of } \overline{p_j p_{j+1}}). \tag{16}$$

Clearly, Eq. (14) is derived from the definition of Cauchy principal value. Secondly, for evaluating the integral I_2, we use the following result:

$$L_1(t,t_o) = -\frac{1}{t-t_o} + \frac{1}{\bar{t}-\bar{t}_o}\frac{\mathrm{d}\bar{t}}{\mathrm{d}t} = -\frac{1}{|t-\mathrm{t}_o|\mathrm{e}^{i\,\alpha_j}} + \frac{1}{|t-t_o|\mathrm{e}^{-i\,\alpha_j}}\frac{\mathrm{e}^{-i\,\alpha_j}}{\mathrm{e}^{i\,\alpha_j}} = 0,$$
$$\text{(for } t_o \text{ at middle point of } \overline{p_j p_{j+1}}\text{)}. \tag{17}$$

Similarly, we have

$$L_2(t,t_o) = \frac{1}{\bar{t}-\bar{t}_o} - \frac{t-t_o}{(\bar{t}-\bar{t}_o)^2}\frac{\mathrm{d}\bar{t}}{\mathrm{d}t} = 0, \quad \text{(for } t_o \text{ at middle point of } \overline{p_j p_{j+1}}\text{)}. \tag{18}$$

In the meantime, for the right-hand side of Eq. (1), in the condition of $Q(t)$ being constant along Γ_j, we have

$$I_4 = \int_{\Gamma_j} \ln|t-t_o|\,\mathrm{d}t = 2\mathrm{e}^{i\alpha_j}\int_0^{d_j} \ln s\,\mathrm{d}s = 2\mathrm{e}^{i\alpha_j} d_j(\ln d_j - 1),$$
$$\text{(for } t_o \text{ at middle point of } \overline{p_j p_{j+1}}\text{)}, \tag{19}$$

$$I_5 = \int_{\Gamma_j} \frac{t-t_o}{\bar{t}-\bar{t}_o}\mathrm{d}\bar{t} = 2\mathrm{e}^{i\alpha_j}\int_0^{d_j} \mathrm{d}s = 2\mathrm{e}^{i\alpha_j} d_j,$$
$$\text{(for } t_o \text{ at middle point of } \overline{p_j p_{j+1}}\text{)}. \tag{20}$$

In the second case, t_o is placed at the middle point of the interval $\overline{p_k p_{k+1}}$ and integration is performed along $\overline{p_j p_{j+1}}$ denoting by Γ_j (Fig. 3). For the left and right-hand side of Eq. (1), in the condition of $U(t)$ and $Q(t)$ being constant along Γ_j, we meet the following integrals:

$$J_1 = \int_{\Gamma_j} \frac{\mathrm{d}t}{t-t_\mathrm{o}}, \qquad J_2 = \int_{\Gamma_j} L_1(t,t_o)\mathrm{d}t, \qquad J_3 = \int_{\Gamma_j} L_2(t,t_o)\mathrm{d}t,$$
$$J_4 = \int_{\Gamma_j} \ln|t-t_o|\,\mathrm{d}t, \qquad J_5 = \int_{\Gamma_j} \frac{t-t_o}{\bar{t}-\bar{t}_o}\mathrm{d}\bar{t}, \quad \text{(for } t_o \text{ at middle point of } \overline{p_k p_{k+1}}\text{)}. \tag{21}$$

Those integrals can be evaluated numerically, saying by using Simpson's rule. All integrals in Eq. (21) are regular.

Similarly, for the exterior problem shown by Fig. 2d, after discretization of Eq. (5), the relevant BIE can be reduced to the following form

$$[\mathbf{D}_2]\{\{d\} - \{d_o\}\} = [\mathbf{Q}_2]\{\{q\} - \{q_o\}\}. \tag{22}$$

It is seen that two matrices $[\mathbf{D}_2]$ and $[\mathbf{Q}_2]$ are formulated based on Eq. (5) and two elastic constants G_2 and ν_2.

It is known that the matrix $[\mathbf{D}_2]$ is invertible [18]. Thus, from Eq. (22), we have

$$\{d\} = [\mathbf{D}_2^{-1}][\mathbf{Q}_2]\{q\} - [\mathbf{D}_2^{-1}][\mathbf{Q}_2]\{q_o\} + \{d_o\}. \tag{23}$$

Substituting Eq. (23) into Eq. (13) yields

$$[\mathbf{C}]\{q\} = \{h_o\}, \tag{24}$$

where

$$[\mathbf{C}] = [\mathbf{D}_1]\,[\mathbf{D}_2^{-1}]\,[\mathbf{Q}_2] - [\mathbf{Q}_1], \tag{25}$$
$$\{h_o\} = [\mathbf{D}_1]\,[\mathbf{D}_2^{-1}][\mathbf{Q}_2]\{q_o\} - [\mathbf{D}_1]\{d_o\}. \tag{26}$$

After obtaining $\{q\}$ from the solution of algebraic equation (24), the vector $\{d\}$ can be evaluated by Eq. (23).

For evaluating the hoop stress σ_T, the following technique is suggested [19]. In fact, in the plane strain case, the strain component ε_T (in T-direction) can be expressed as (Fig. 2)

$$\varepsilon_T = \frac{1}{2G(1+\nu)}(\sigma_T(1-\nu^2) - \nu(1+\nu)\,\sigma_N), \tag{27}$$

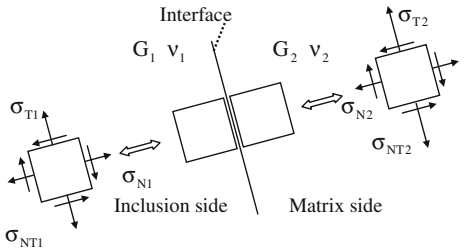

Fig. 4 Stress components at the inclusion and matrix sides

or

$$\sigma_T = \frac{2G(1+\nu)\,\varepsilon_T + \nu(1+\nu)\,\sigma_N}{1-\nu^2}. \tag{28}$$

In Eq. (28), the component σ_N is from input datum, and ε_T is the strain in the T-direction, which can be evaluated from the numerical solution of displacements along the boundary. In fact, the elongation of a boundary element can be found from the displacement solution, and the strain ε_T can be evaluated accordingly. Thus, the values of σ_T at many discrete points along the boundary can be evaluated.

For the stress and strain components at two sides of interface (Fig. 4), the following results need to emphasize. Clearly, we have the following equalities:

$$\sigma_{N1} = \sigma_{N2}, \quad \sigma_{NT1} = \sigma_{NT2}, \tag{29}$$

where σ_{N1}, σ_{NT1} and σ_{N2}, σ_{NT2} denote the stress components at the inclusion side and matrix side, respectively. Equation (29) is solely derived from the reciprocity of traction along the interface. Secondly, we have

$$\varepsilon_{T1} = \varepsilon_{T2}, \tag{30}$$

where ε_{T1} and ε_{T2} denote the normal strain component in T-direction at the inclusion side and matrix side, respectively. Equation (30) is solely derived from the fact that displacements are continuous at both sides of the interface.

From Eq. (28), we can get

$$\sigma_{T1} = \frac{2G_1(1+\nu_1)\,\varepsilon_{T1} + \nu_1(1+\nu_1)\,\sigma_{N1}}{1-\nu_1^2}, \quad \text{(at the inclusion side)}, \tag{31}$$

$$\sigma_{T2} = \frac{2G_2(1+\nu_2)\,\varepsilon_{T2} + \nu_2(1+\nu_2)\,\sigma_{N2}}{1-\nu_2^2}, \quad \text{(at the matrix side)}. \tag{32}$$

In Eqs. (31) and (32), $\sigma_{N1} = \sigma_{N2}$, $\varepsilon_{T1} = \varepsilon_{T2}$, and $G_1 \neq G_2$, $\nu_1 \neq \nu_2$. Thus, from Eqs. (31) and (32), we have the inequality

$$\sigma_{T1} \neq \sigma_{T2}\,. \tag{33}$$

In a particular case of $G_1 \neq G_2$ and $\nu_1 = \nu_2$, from Eqs. (31) and (32), one has

$$\sigma_{T2} - \sigma_{T1} = \frac{2(G_2 - G_1)\,\varepsilon_{T1}}{1-\nu_1}. \tag{34}$$

Similarly, we can derive the following inequalities:

$$\varepsilon_{N1} \neq \varepsilon_{N2}, \quad \gamma_1 \neq \gamma_2, \tag{35}$$

where ε_{N1}, ε_{N2} and γ_1, γ_2 denote the normal strain in N-direction and the shear strain, respectively. Strain interface jump conditions were derived in two or three dimensions for bonded and slipping inclusions [20].

The above-mentioned derivation provides one possibility by using some substitutions. We can propose a second substitution technique. It is known that if the real size is different from degenerate scale, the matrix $[\mathbf{Q}_2]$ is invertible [21–23]. Thus, from Eq. (22), we have

$$\{q\} = [\mathbf{Q}_2^{-1}][\mathbf{D}_2]\{\{d\} - \{d_o\}\} + \{q_o\}. \tag{36}$$

Substituting Eq. (36) into Eq. (13) yields

$$[\mathbf{C}]\{d\} = \{h_o\}, \tag{37}$$

where

$$[\mathbf{C}] = [\mathbf{Q}_1][\mathbf{Q}_2^{-1}][\mathbf{D}_2] - [\mathbf{D}_1], \tag{38}$$

$$\{h_o\} = [\mathbf{Q}_1][\mathbf{Q}_2^{-1}][\mathbf{D}_2]\{d_o\} - [\mathbf{Q}_1]\{q_o\}. \tag{39}$$

After obtaining $\{d\}$ from the solution of algebraic equation (37), the vector $\{q\}$ can be evaluated by Eq. (36).

In addition, we can propose the third substitution technique. It is known that if the real size is different to degenerate scale, the matrix $[\mathbf{Q}_1]$ is invertible [21–23]. Thus, from Eq. (13), we have

$$\{q\} = [\mathbf{Q}_1^{-1}][\mathbf{D}_1]\{d\}. \tag{40}$$

Substituting Eq. (40) into Eq. (22) yields

$$[\mathbf{C}]\{d\} = \{h_o\}, \tag{41}$$

where

$$[\mathbf{C}] = [\mathbf{Q}_2][\mathbf{Q}_1^{-1}][\mathbf{D}_1] - [\mathbf{D}_2], \tag{42}$$

$$\{h_o\} = -[\mathbf{D}_2]\{d_o\} + [\mathbf{Q}_2]\{q_o\}. \tag{43}$$

After obtaining $\{d\}$ from the solution of algebraic equation (41), the vector $\{q\}$ can be evaluated by Eq. (40). It is noted here that one type of similar substitution has been suggested by Dong et. al. [3].

In fact, three suggested approaches in solving the system of linear equations are well known. The purpose for the suggested three variations of substitution is to provide flexibility in the numerical solution.

It is found from the first numerical example cited below that the three schemes of substitution provide the same computed results. In this case, we can use any substitution scheme in a real computation. For example, we can use the first one in the problem, which is expressed by Eqs. (13), (22)–(26).

2.3 Elastic inclusion with an applied concentrated force

The original problem for an elastic inclusion is shown by Fig. 5o, where the inclusion and matrix have the elastic constants G_1, ν_1 and G_2, ν_2, respectively. In addition, there is a concentrated force "P" applied on the elastic inclusion.

The original problem shown by Fig. 5o can be decomposed into two boundary value problems (Fig. 5a, b). Among them, one is exterior BVP shown by Fig. 5a and the other is the interior BVP shown by Fig. 5b. Clearly, from the continuation condition of displacements and reciprocal property of tractions along interface boundary, the same vectors $\{d\}$ and $\{q\}$ are applied along the boundary in Fig. 5a and b.

For the exterior BVP shown by Fig. 5a, after discretization of Eq. (5), the relevant BIE can be reduced to the form

$$[\mathbf{D}_2]\{d\} = \quad [\mathbf{Q}_2]\{q\}. \tag{44}$$

It is seen that two matrices $[\mathbf{D}_2]$ and $[\mathbf{Q}_2]$ are formulated based on Eq. (5) and two elastic constants G_2 and ν_2.

The situation in the present case has some differences with that studied in Sect. 2.2. In Fig. 5b, the boundary traction, or the vector $\{q\}$ is not self-equilibrium, but it is in equilibrium with the concentrated force "P".

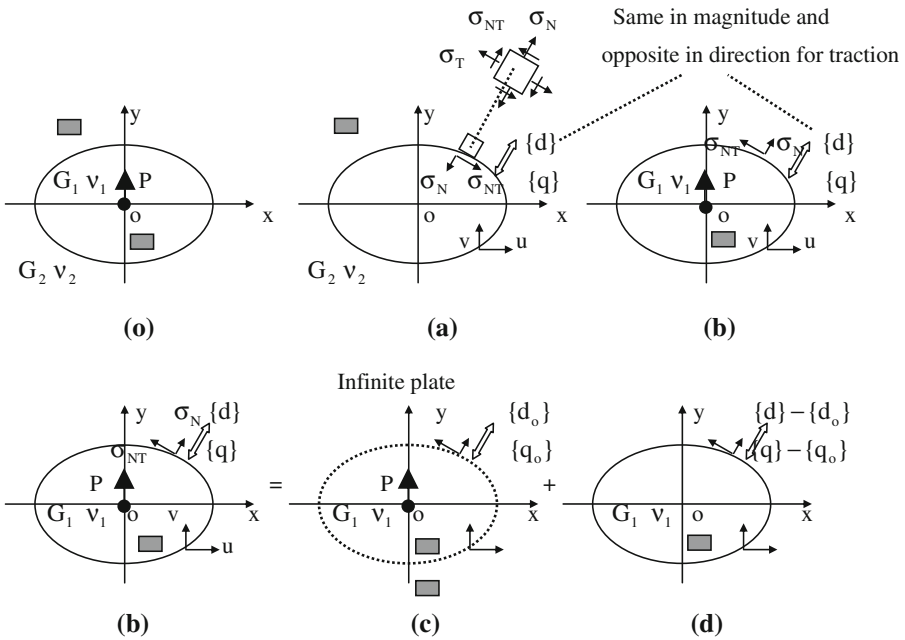

Fig. 5 An infinite plate with an elastic inclusion and a concentrated force P, **o** the original problem, **a** an exterior BVP, **b** an interior BVP, **c** a homogenous infinite plate with a concentrated force P, **d** an particular interior BVP (where (**b**)=(**c**)+(**d**)), *filled rectangle* region defined

Naturally, the interior BVP by Fig. 5b can be considered as a superposition of two problems shown by Fig. 5c, d. In the problem shown by Fig. 5c, a homogenous infinite plate is applied by a concentrated force "P". For this problem, the following complex potentials were available [24]

$$\phi(z) = -\frac{\mathrm{Pi}}{2\,\pi(\kappa+1)}\ln z, \quad \phi(z) = -\frac{\kappa\,\mathrm{Pi}}{2\,\pi(\kappa+1)}\ln z. \tag{45}$$

Those complex potentials correspond to a concentrated force "P" applied at the origin.

Those complex potentials (or $\phi(z)$ and $\psi(z)$) cause some displacement vector $\{d_o^*\}$ and traction vector $\{q_o^*\}$ along the boundary. Along the boundary with dashed line in Fig. 5c, we can assume the displacement vector $\{d_o\}$ (where $\{d_o\} = -\{d_o^*\}$) and traction vector $\{q_o\}$ (where $\{q_o\} = -\{q_o^*\}$). Therefore, the traction vector $\{q_o\}$ is now in equilibrium with the concentrated force "P" (Fig. 5c).

Clearly, after using the principle of superposition, the displacement vector is $\{d\} - \{d_o\}$ and traction vector is $\{q\} - \{q_o\}$ in Fig. 5d. Clearly, since the traction vector $\{q\} - \{q_o\}$ applied on the boundary is in self-equilibrium, we can use the BIE for interior BVP between the displacement vector $\{d\} - \{d_o\}$ and the traction vector $\{q\} - \{q_o\}$ accordingly. After discretization of Eq. (1), the relevant BIE can be reduced to the following form

$$[\mathbf{D}_1]\{\{d\} - \{d_o\}\} = [\mathbf{Q}_1]\{\{q\} - \{q_o\}\}. \tag{46}$$

It is seen that two matrices $[\mathbf{D}_1]$ and $[\mathbf{Q}_1]$ are formulated based on Eq. (1) and two elastic constants G_1 and ν_1.

It is known that the matrix $[\mathbf{D}_2]$ is invertible. Thus, from Eq. (44), we have

$$\{d\} = \quad [\mathbf{D}_2^{-1}][\mathbf{Q}_2]\,\{q\}. \tag{47}$$

Substituting Eq. (47) into Eq. (46) yields

$$[\mathbf{C}]\{q\} = \{h_o\}, \tag{48}$$

where

$$[\mathbf{C}] = [\mathbf{D}_1][\mathbf{D}_2^{-1}][\mathbf{Q}_2] - [\mathbf{Q}_1], \tag{49}$$

$$\{h_o\} = [\mathbf{D}_1]\{d_o\} - [\mathbf{Q}_1]\{q_o\}. \tag{50}$$

After obtaining $\{q\}$ from the solution of algebraic equation (48), the vector $\{d\}$ can be evaluated by Eq. (47).

3 Numerical examples

Several numerical examples are provided to prove the efficiency of the suggested method. In all numerical examples, the plane strain condition and $\nu_1 = \nu_2 = 0.3$ are assumed.

Example 1 The first example is devoted to evaluate the displacement and stress components u, v, σ_N, σ_{NT} and σ_T along the boundary of an elastic inclusion (Fig. 6a). The elliptic inclusion with the elastic properties G_1 and ν_1 is embedded in an infinite medium with the elastic properties G_2 and ν_2. The elliptic inclusion with two half-axes "a" and "b" and the infinite plate has the remote loading $\sigma_y^\infty = p$. The boundary of the inclusion is defined by

$$x = a\cos\theta, \quad y = b\sin\theta, \qquad (0 \le \theta \le 2\pi). \tag{51}$$

In the computation, $N = 90$ divisions are used for the angle θ ($0 \le \theta \le 2\pi$). The displacements and tractions are assumed to be constant along all boundary elements.

For the following cases: $b/a = 0.5$, $G_1/G_2 = 10^{-5}$, 0.1, 0.5, 1, 2 and 10, and $0 \le \theta \le 2\pi$, the computed results for stresses σ_N and σ_{NT} along the interface and σ_T at matrix side are expressed as (Fig. 6a)

$$\sigma_N = f_1(G_1/G_2, \theta)p, \quad \sigma_{NT} = f_2(G_1/G_2, \theta)p, \quad \sigma_T = f_3(G_1/G_2, \theta)p. \tag{52}$$

The computed non-dimensional stresses for $f_1(=\sigma_N/p)$, $f_2(=\sigma_{NT}/p)$ and $f_3(=\sigma_T/p)$ are plotted in Figs. 7, 8 and 9, respectively.

From the plotted results, we see that, when $G_1/G_2 = 10^{-5}$, $\sigma_N/p \approx 0$ and $\sigma_{NT}/p \approx 0$ for all $0 \le \theta \le 2\pi$. This result is reasonable because of no resistance for deformation of elastic inclusion when $G_1/G_2 \approx 0$ (or $G_1/G_2 = 10^{-5}$). In addition, when $G_1/G_2 = 10^{-5}$, we have the hoop stress $\sigma_T/p = 4.995$ for $\theta = 0$. It is known that for an elliptic notch with $b/a = 0.5$ and traction-free condition along the boundary (or $G_1/G_2 = 0$, or $G_1 = 0$), the stress concentration factor is equal to "5". This fact (or $4.995 \approx 5$) means that higher accuracy has been achieved in computation. Secondly, at the crown point of the elliptic notch (or $\theta = 0$, or $x = a$ and $y = 0$), we have $\sigma_T/p = 4.995$, 3.534, 1.665, 0.996, 0.524, and 0.020 for $G_1/G_2 = 10^{-5}$, 0.1, 0.5, 1, 2, 10, respectively. That is to say a weaker elastic inclusion (or $G_1/G_2 = 10^{-5}$, or $G_1/G_2 \approx 0$) will cause a higher stress concentration for the notched plate.

In the example, we have checked numerically that the three schemes of substitution provide the same computed results.

Example 2 In the second example, a concentrated force "P" in y-direction is applied at the elliptic inclusion (Fig. 6b). The theoretical derivation for this problem has been introduced in Sect. 2.3. Except for the loading condition, all the conditions in the second example are same as in the first example.

For the following cases: $b/a = 0.5$, $G_1/G_2 = 10^{-5}$, 0.1, 0.5, 1, 2 and 10, and $0 \le \theta \le 2\pi$. The computed results for stresses σ_N and σ_{NT} along the interface and σ_T at matrix side are expressed as (Fig. 6b)

$$\sigma_N = g_1(G_1/G_2, \theta)\frac{P}{2a}, \quad \sigma_{NT} = g_2(G_1/G_2, \theta)\frac{P}{2a}, \quad \sigma_T = g_3(G_1/G_2, \theta)\frac{P}{2a}. \tag{53}$$

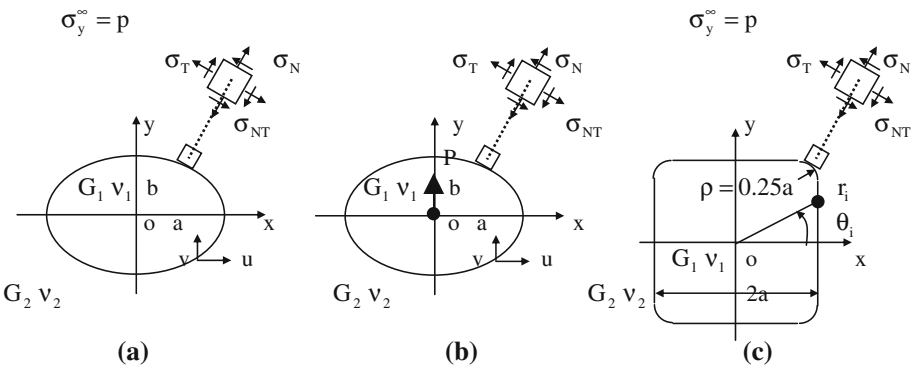

Fig. 6 **a** An elliptic inclusion with elastic constants (G_1 ν_1) embedded in infinite matrix with elastic constants (G_2 ν_2) in the case of remote loading $\sigma_y^\infty = p$, **b** an elliptic inclusion with elastic constants (G_1 ν_1) embedded in infinite matrix with elastic constants (G_2 ν_2) in the case of a concentrated force "P", **c** a square notch with rounded corners and elastic constants (G_1 ν_1) embedded in infinite matrix with elastic constants (G_2 ν_2) in the case of remote loading $\sigma_y^\infty = p$

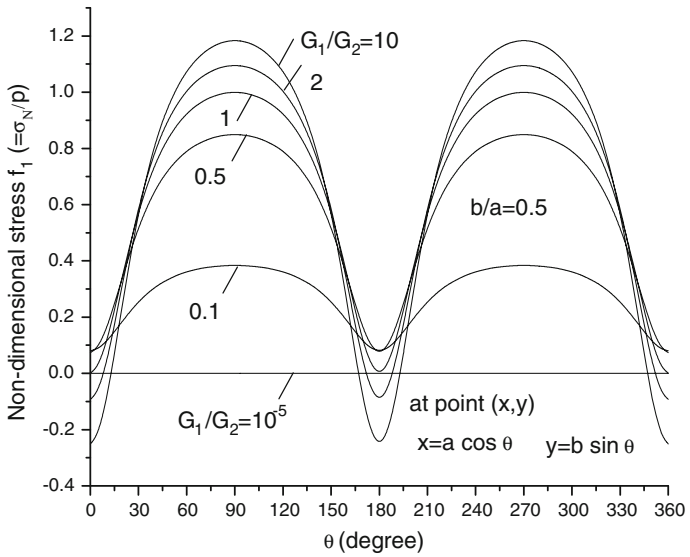

Fig. 7 Non-dimensional normal contact stress $f_1(G_1/G_2, \theta)(= \sigma_N /p)$ along the elliptic interface under a remote loading $\sigma_y^\infty = p$ (see Eq. (52) and Fig. 6a)

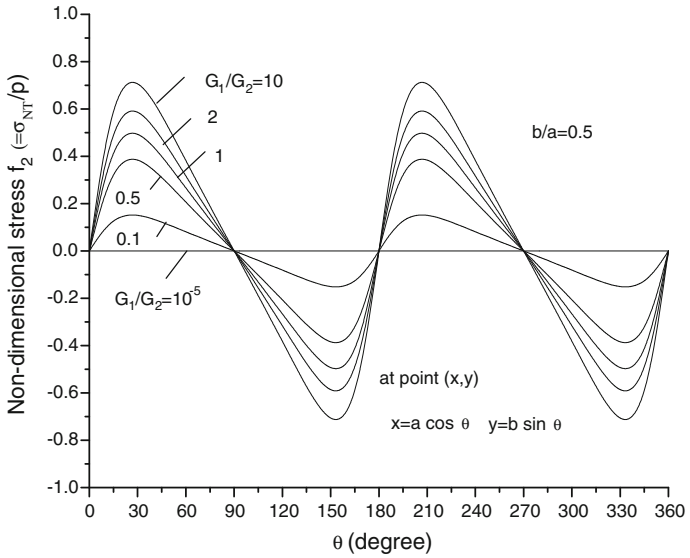

Fig. 8 Non-dimensional shear contact stress $f_2(G_1/G_2, \theta)(= \sigma_{NT} /p)$ along the elliptic interface under a remote loading $\sigma_y^\infty = p$ (see Eq. (52) and Fig. 6a)

The computed non-dimensional stresses for $g_1(= \sigma_N /(P/2a))$, $g_2(= \sigma_{NT} /(P/2a))$, and $g_3(= \sigma_T /(P/2a))$ are plotted in Figs. 10, 11 and 12, respectively.

From the plotted results, we see that the stress distributions in the present example are quite different from those in the first example. For example, the hoop stress component σ_T is not dominant in the present case. For example, for $G_1/G_2 = 10^{-5}$, $g_3(G_1/G_2, \theta)_{\max} = 0.339$ $(= \sigma_T /(P/2a))$ at the angles $\theta = 24°$ and $\theta = 156°$. In addition, a weaker elastic inclusion will cause a sharp distribution for the stress component σ_N. For example, for $G_1/G_2 = 10^{-5}$, $g_1(G_1/G_2, \theta)(= \sigma_N /(P/2a))$ changes from -1.447 $(\theta = 90°)$, 0 $(\theta = 180°)$ to 1.447 $(\theta = 270°)$. However, for $G_1/G_2 = 10$, $g_1(G_1/G_2, \theta)$ $(= \sigma_N /(P/2a))$ changes from -0.570 $(\theta = 90°)$, 0 $(\theta = 180°)$ to 0.570 $(\theta = 270°)$.

Example 3 The third example is devoted to evaluate the displacement and stress components u, v, σ_N, σ_{NT}, and σ_T along the boundary of a square inclusion with a small rounded corner $\rho = 0.25a$ (Fig. 6c). The inclusion has the remote loading $\sigma_y^\infty = p$ (Fig. 6c). All conditions in the third example are same as in the first example.

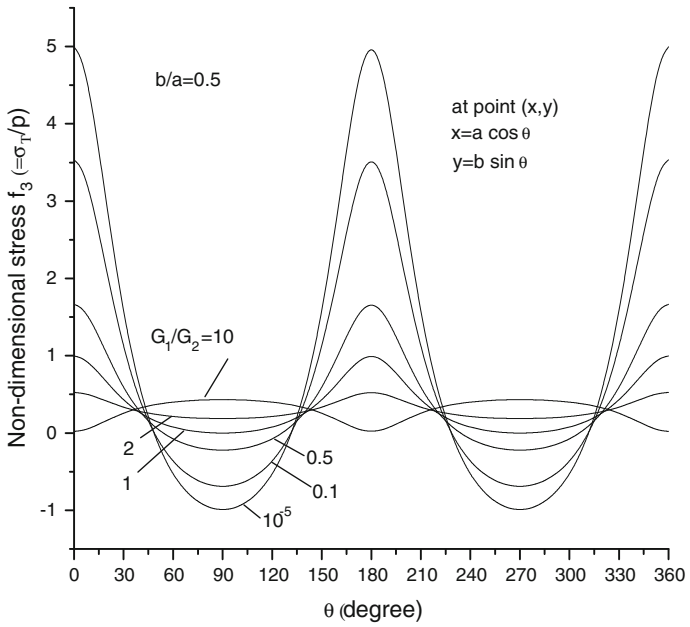

Fig. 9 Non-dimensional hoop stress $f_3(G_1/G_2, \theta)(= \sigma_T / p)$ along the elliptic interface under a remote loading $\sigma_y^{\infty} = p$ (see Eq. (52) and Fig. 6a)

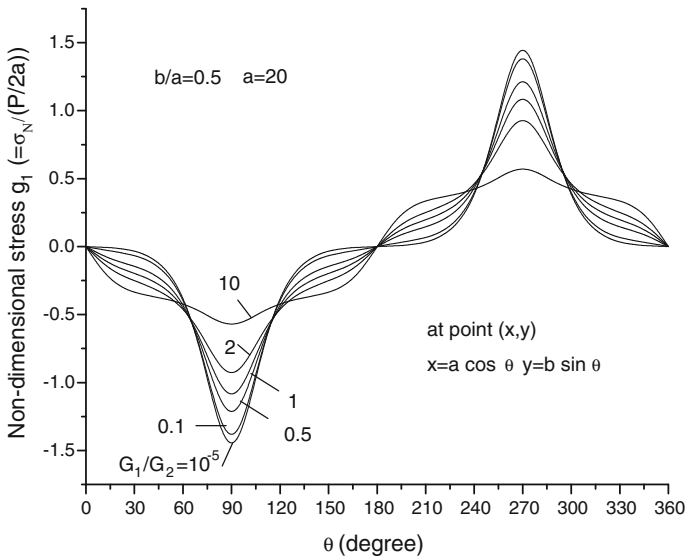

Fig. 10 Non-dimensional normal contact stress $g_1(G_1/G_2, \theta)(= \sigma_N / (P/2a))$ along the elliptic interface under a concentrated force "P" (see Eq. (53) and Fig. 6b)

The boundary of the inclusion is defined by

$$x = r_i \cos\theta_i, \quad y = r_i \sin\theta_i, \quad (0 \le \theta_i \le 2\,\pi). \tag{54}$$

For the following cases: $G_1/G_2 = 10^{-5}$, 0.1, 0.5, 1, 2 and 10, and $0 \le \theta \le 2\,\pi$, the computed results for stresses σ_N and σ_{NT} along the interface and σ_T at matrix side are expressed as (Fig. 6c)

$$\sigma_N = h_{1(G_1/G_2,\theta)p}, \quad \sigma_{NT} = h_2(G_1/G_2, \theta)p, \quad \sigma_T = h_3(G_1/G_2, \theta)p. \tag{55}$$

The computed non-dimensional stresses for $h_1(= \sigma_N / p)$, $h_2(= \sigma_{NT} / p)$, and $h_3(= \sigma_T / p)$ are plotted in Figs. 13, 14, and 15, respectively.

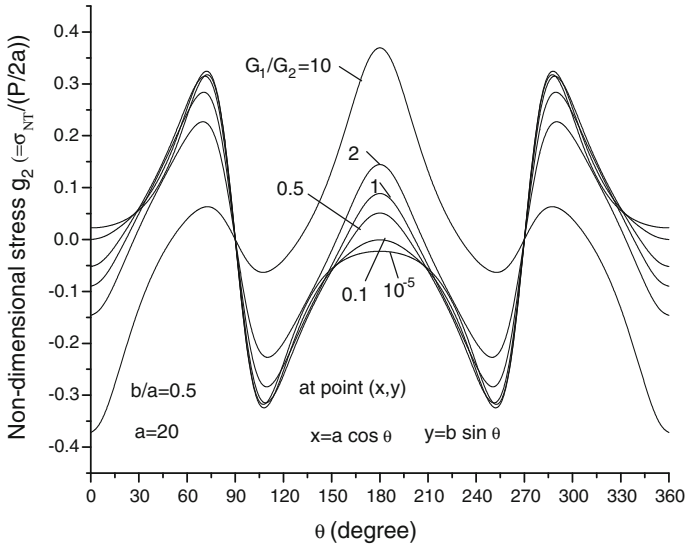

Fig. 11 Non-dimensional shear contact stress $g_2(G_1/G_2, \theta)(= \sigma_{NT}/(P/2a))$ along the elliptic interface under a concentrated force "P" (see Eq. (53) and Fig. 6b)

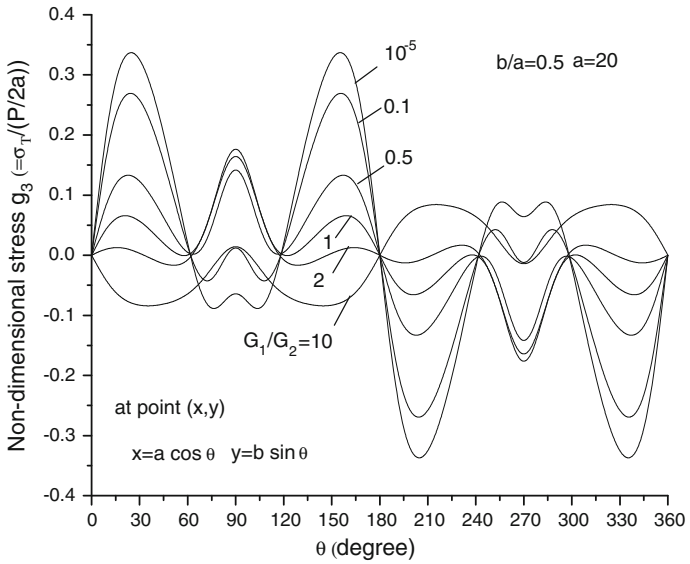

Fig. 12 Non-dimensional hoop stress $g_3(G_1/G_2, \theta)(= \sigma_T/(P/2a))$ along the elliptic interface under a concentrated force "P" (see Eq. (53) and Fig. 6b)

From the plotted results, we see that, when $G_1/G_2 = 10^{-5}$, $\sigma_N/p \approx 0$ and $\sigma_{NT}/p \approx 0$ for all $0 \le \theta \le 2\pi$. This result is reasonable because of no resistance for deformation of elastic inclusion when $G_1/G_2 \approx 0$ (for $G_1/G_2 = 10^{-5}$). However, for a rigid inclusion case of $G_1/G_2 = 10$, we have the maximum $\sigma_N/p = 1.484$ at $\theta = 52^\circ$ and the maximum $\sigma_{NT}/p = 1.054$ at $\theta = 44^\circ$, which is a point at the corner portion (Fig. 6c).

For $G_1/G_2 = 10^{-5}$, it is nearly to the case of no inclusion, or the notch contour is traction-free. In this case, we find stress concentration at the corner portion. For example, we have the maximum $\sigma_T/p = 3.341$ at $\theta = 40^\circ$.

4 Conclusions

Based on a complex variable boundary integral equation (CVBIE) suggested previously [8], this paper provides a numerical solution for elastic inclusion problem using CVBIE. There are some slight differences between

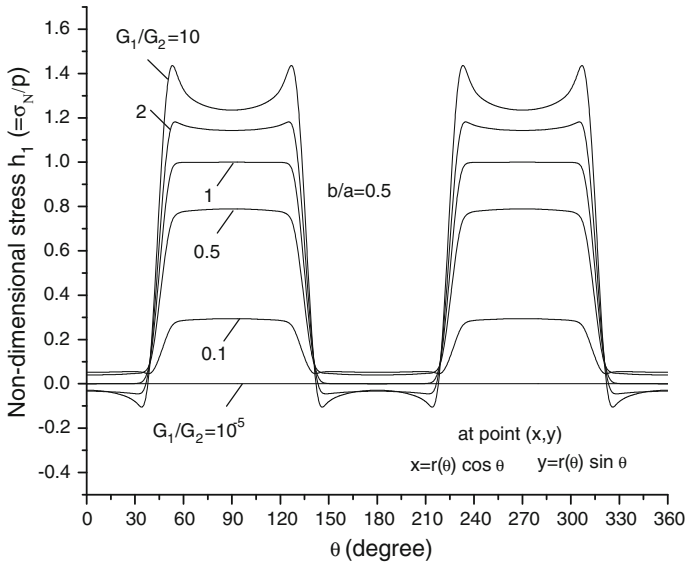

Fig. 13 Non-dimensional normal contact stress $h_1(G_1/G_2, \theta)(= \sigma_N / p)$ along the rounded square interface under a remote loading $\sigma_y^{\infty} = p$ (see Eq. (55) and Fig. 6c)

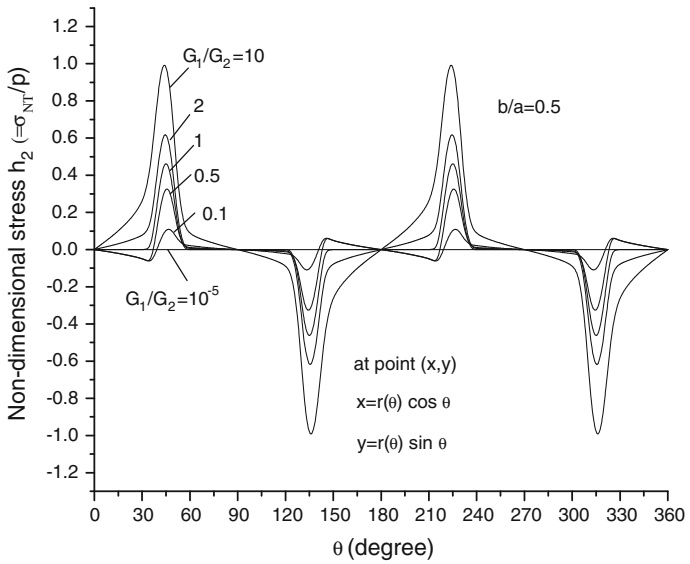

Fig. 14 Non-dimensional shear contact stress $h_2(G_1/G_2, \theta)(= \sigma_{NT} / p)$ along the rounded square interface under a remote loading $\sigma_y^{\infty} = p$ (see Eq. (55) and Fig. 6c)

Ref. [8] and the present paper. In Ref. [8], the remote loading in the exterior BVP should be vanishing, and in this paper, the remote loading is not vanishing. Secondly, in Ref. [8], one studies the medium with homogenous elastic property, and in present paper, one should connect two BIEs for the interior region and the exterior region with different elastic constants together.

The formulation based on the suggested CVBIE is presented in a straightforward manner. For example, the first term in the left-hand side of Eq. (1) belongs to a Cauchy singular integral that is well defined in many textbooks. Naturally, only if one knows the structures of kernels in BIE very well, one can propose the effective scheme in discretization. Comparatively speaking, the formulation in this paper is effective. For example, all deviations and computations were based on two BIEs Eqs. (1) and (5), which are for the interior and exterior BVPs. In addition, we have used the properties of some integration operators accordingly. Therefore, a flexible solution technique was provided. Particularly, as claimed above, there is no limitation for the shape of interface boundary.

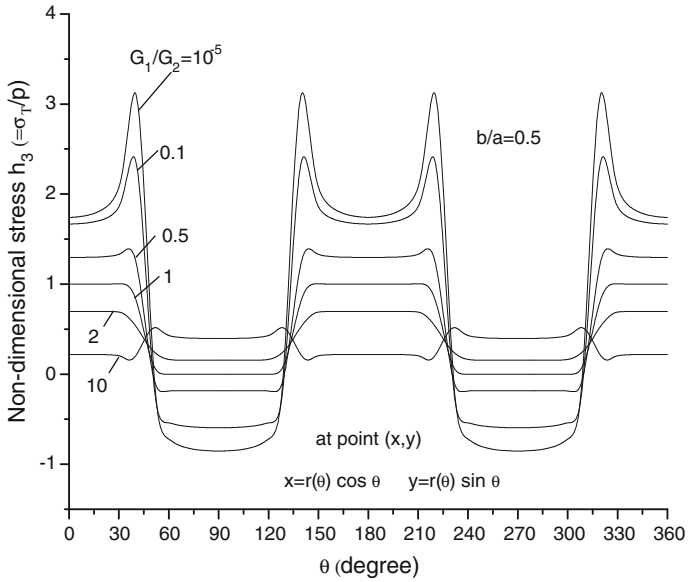

Fig. 15 Non-dimensional hoop stress $h_3(G_1/G_2, \theta)(= \sigma_T / p)$ along the rounded square interface under a remote loading $\sigma_y^{\infty} = p$ (see Eq. (55) and Fig. 6c)

References

1. Chang, C.S., Conway, H.D.: Stress analysis of an infinite plate containing an elastic rectangular inclusion. Acta Mech. **8**, 160–173 (1969)
2. Dong, C.Y., Lo, S.H, Cheung, Y.K.: Application of the boundary-domain integral equation in elastic inclusion problems. Eng. Anal. Bound. Elem. **26**, 471–477 (2002)
3. Dong, C.Y., Lo, S.H., Cheung, Y.K.: Numerical solution for elastic half-plane inclusion problems by different integral equation approaches. Eng. Anal. Bound. Elem. **28**, 123–130 (2004)
4. Dong, C.Y., Lee, K.Y.: A new integral equation formulation of two-dimensional inclusion–crack problems. Int. J. Solids Struct. **42**, 5010–5020 (2005)
5. Legros, B., Mogilevskaya, S.G., Crouch, S.L.: A boundary integral method for multiple circular inclusions in an elastic half-plane. Eng. Anal. Bound. Elem. **28**, 1083–1098 (2004)
6. Luo, J.C., Gao, C.F.: Faber series method for plane problems of an arbitrarily shaped inclusion. Acta Mech. **208**, 133–145 (2009)
7. Chen, J.T., Lee, Y.T.: Torsional rigidity of a circular bar with multiple circular inclusions using the null-field integral approach. Comput. Mech. **44**, 221–232 (2009)
8. Chen, Y.Z., Lin, X.Y.: Dual boundary integral equation formulation in plane elasticity using complex variable. Eng. Anal. Bound. Elem. **34**, 834–844 (2010)
9. Brebbia, C.A., Tells, J.C.F., Wrobel, L.C.: Boundary Element Techniques—Theory and Application in Engineering. Springer, Heidelberg (1984)
10. Cheng, A.H.D., Cheng, D.S.: Heritage and early history of the boundary element method. Eng. Anal. Bound. Elem. **29**, 286–302 (2005)
11. Chen, J.T., Liang, M.T., Yang, S.S.: Dual boundary integral equations for exterior problems. Eng. Anal. Bound. Elem. **16**, 333–340 (1995)
12. Chen, J.T., Chen, Y.W.: Dual boundary element analysis using complex variables for potential problems with or without a degenerate boundary. Eng. Anal. Bound. Elem. **24**, 671–684 (2000)
13. Chen, Y.Z., Wang, Z.X.: Dual boundary integral equation formulation in antiplane elasticity using complex variable. Comput. Mech. **45**, 167–178 (2010)
14. Kolte, R., Ye, W., Hui, C.Y., Mukherjee, S.: Complex variable formulations for usual and hypersingular integral equations for potential problems—with applications to corners and cracks. Comput. Mech. **17**, 279–286 (1996)
15. Linkov, A.M.: Boundary Integral Equations in Elasticity. Kluwer, Dordrecht (2002)
16. Mogilevskaya, S.G., Linkov, A.M.: Complex fundamental solutions and complex variables boundary element method in elasticity. Comput. Mech. **22**, 88–92 (1998)
17. Mogilevskaya, S.G.: Complex hypersingular integral equation for the piecewise homogeneous half-plane with cracks. Int. J. Fract. **102**, 177–204 (2004)
18. Chen, Y.Z, Wang, Z.X., Lin, X.Y.: A new kernel in BIE and the exterior boundary value problem in plane elasticity. Acta Mech. **206**, 207–224 (2009)
19. Chen, Y.Z., Wang, Z.X.: Solution for hole problems of elastic half-plane with gravity force using boundary integral equation. Int. J. Rock Mech. Min. Sci. **48**, 520–526 (2011)

20. Markenscoff, X.: A note on strain jump conditions and Cesáro integrals for bonded and slipping inclusions. J. Elast. **45**, 45–51 (1996)
21. Chen, J.T., Kuo, S.R., Lin, J.H.: Analytical study and numerical experiments for degenerate scale problems in the boundary element method of two-dimensional elasticity. Int. J. Numer. Methods Eng. **54**, 1669–1681 (2002)
22. Vodcka, R., Mantic, V.: On invertibility of elastic single-layer potential operator. J. Elast. **74**, 147–173 (2004)
23. Vodcka, R., Mantic, V.: On solvability of a boundary integral equation of the first kind for Dirichlet boundary value problems in plane elasticity. Comput. Mech. **41**, 817–826 (2008)
24. Muskhelishvili, N.I.: Some Basic Problems of Mathematical Theory of Elasticity. Noordhoof, Groningen (1963)